Table 2 Comparison with Rogers[2]; $Pr = 0.723$, $\omega = 1.0$, $g_0 = 0.2$

	Our calculations						Rogers[2]
E	0.0	0.15	0.50	0.90	0.95	1.0	1.0
$-\beta$	0.33336	0.33383	0.33501	0.33641	0.33658	0.33676	0.336754

properties when calculating separating flows. Figure 1 shows the influence of improved viscosity-enthalpy relations for an ideal gas as well as solutions using N. B. Cohen's[7] properties for real air. Also, solutions generated with simplified gas properties can exhibit incorrect trends as shown in Fig. 2. The separation value of β generally increases with E for gases with realistic values of ω, the converse is true for $\omega = 1.0$. The generally higher values of β required to obtain separation for real air result from the lower densities caused by dissociation. As shown in Fig. 3, the dimensionless displacement thickness δ^* initially increases as suction is applied to high-Mach number flows, an effect not observed in low-speed flows. The decreasing influence of wall temperature as suction is applied is also evident. In the hypersonic limit δ^* is infinite, thus, Rogers[2] has to compute

$$I_1 \equiv (1 - E)\delta^* = \int_0^\infty (g - f'^2)d\eta$$

But as seen from Table 3, the hypersonic limit value of $(1 - E)\delta^*$ has restricted applicability, particularly in view of the nonmonotonic behavior of $(1 - E)\delta^*$ for $\omega \neq 1.0$. Finally, Fig. 4 shows the marked difference between our velocity profiles and those of Rogers.[2]

In summary we have shown, through a few tables and figures, that the arguments over accuracy entered into by Rogers[3] are quite academic as the data in question resembles physical reality rather poorly. At most, Rogers might have suggested that Fox and Saland[4] limit their extensive tabulations to the number of assured significant figures. Our purpose was not to present comprehensive data relating to laminar separating boundary layers. Greater significance is attached to the demonstrated sensitivity of the results to physical properties variation, particularly at high Mach numbers where the variation of the $(\rho\mu)$ product is most pronounced, and when suction is applied to bring the region of most rapid variation close to the wall. Our results also suggest that the more important engineering problem of predicting turbulent separating boundary layers, will be strongly influenced by the choice of turbulent-viscosity model.

Table 3 Displacement thickness $f_0 = 0$, $g_0 = 0.2$

	$(1 - E)\delta^*$			
E	$Pr = 1.0$ $\omega = 1.0$	0.723 1.0	0.723 0.7	0.723 0.5
0	1.406	1.243	1.293	1.337
0.15	1.501	1.342	1.372	1.401
0.50	1.720	1.579	1.523	1.494
0.90	1.971	1.855	1.466	1.259
0.95	2.003	1.891	1.213	1.099
1.0 (Rogers[2])	2.03446	1.93018		

References

[1] Lees, L. and Reeves, B. L., "Supersonic Separated and Reattaching Laminar Flows: I. General Theory and Application of Adiabatic Boundary-Layer/Shock Wave Interactions," *AIAA Journal*, Vol. 2, No. 11, Nov. 1964, pp. 1907–1920.

[2] Rogers, D. F., "Reverse Flow Solutions for Compressible Laminar Boundary-Layer Equations," *The Physics of Fluids*, Vol. 12, No. 3, March 1969, pp. 517–523.

[3] Rogers, D. F., "Comment on 'Separation Solutions for Laminar Boundary Layer,'" *AIAA Journal*, Vol. 8, No. 11, Nov. 1970, pp. 2107–2109.

[4] Fox, H. and Saland, H., "Separation Studies for the Similar Laminar Boundary Layer," *AIAA Journal*, Vol. 8, No. 4, April 1970, pp. 780–788.

[5] Libby, P. A. and Liu, T. M., "Some Similar Laminar Flows Obtained by Quasilinearization," *AIAA Journal*, Vol. 6, No. 8, Aug. 1968, pp. 1541–1548.

[6] Wortman, A., "Mass Transfer in Self-Similar Boundary-Layer Flows," Ph.D. dissertation, 1969, School of Engineering and Applied Science, Univ. of California, Los Angeles, Calif.

[7] Cohen, N. B., "Boundary-Layer Similar Solutions and Correlation Equations for Laminar Heat Transfer Distribution in Equilibrium Air at Velocities up to 41,000 Feet per Second," TR R-118, 1961, NASA.

Elastic-Plastic Wave Cancellation in Energy-Absorbing Materials

J. C. S. YANG*

Naval Ordnance Laboratory, Silver Spring, Md.

Introduction

RECENTLY, much interest has been generated in the problems of impact such as those experienced by a vehicle subjected to some high-rate disturbances of the external pressure. These pressure pulses have short duration, a fast rise time followed by an exponential decay, and high intensity which is of sufficient magnitude that may give rise to appreciable stress waves propagating into the interior of the vehicle to cause severe damage or failure to the vehicle or to the various components within the vehicle. Therefore, it becomes necessary to protect the system so that the maximum allowable stress is not exceeded. If the applied load-time curve is considered, the area under this curve represents the impulse or momentum which must be absorbed by the vehicle. Since momentum is conserved, the high-intensity, short-duration pulse must be mitigated to an acceptable stress level for a somewhat longer time. One method of accomplishing this mitigation is to incorporate into the system a material which may be permitted to deform plastically, thereby mitigating the load. The problem has been treated thus far with reasonable success by empirical means, but the intelligent design of such a shock-mitigating system requires the application of the theory of plastic wave propagation, as well as extensive knowledge of the material properties of the mitigating device.

In order to understand this concept, it should be recalled that after a material has been loaded to a point where plastic deformation occurs, while the load is being released, the displacement will obey Hooke's law instead of retracing its original path. Since stress waves will propagate at a speed directly proportional to the square root of the slope of the stress-strain curve, it may be seen that the transmission of stress waves during the unloading will take place much faster than the transmission of the loading stresses above the yield point. Therefore, this method of mitigating the applied impulse is to make use of the overtaking and cancellation of high-intensity plastic stress waves by the faster traveling elastic unloading stress waves (see Fig. 1).

Presented as Paper 70-123 at the AIAA/ASME 12th Structures, Structural Dynamics and Materials Conference, Anaheim Calif., April 19–21, 1971; submitted April 5, 1971; revision received September 1, 1971. This research was supported by the Naval Ordnance Systems Command, ORD-035.

* Research Engineer; presently Associate Professor, Mechanical Engineering Dept., University of Maryland. Member AIAA.

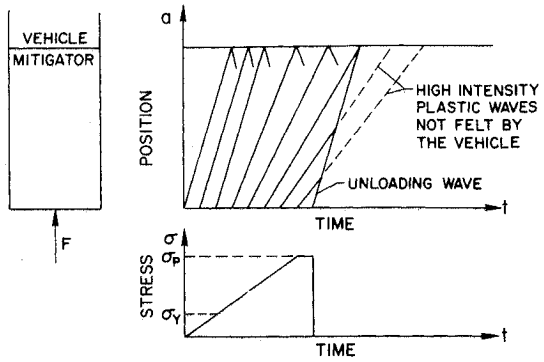

Fig. 1 Wave cancellation.

In this paper the concept of plastic wave cancellation was verified by the comparison of the results of a series of experimental investigations and the predicted results of the one-dimensional strain-rate independent theory of plastic wave propagation. Another experiment was conducted to determine the optimum characteristics of potential mitigating materials. The results indicate that the polymer group, such as Ethocel, Teflon, Lexan, and Polyurethane, is very efficient for shock mitigation from both a weight and volume standpoint. Materials such as these will probably exhibit some strain-rate dependence which must be known before a rational design analysis can be undertaken.

Analysis

The familiar equations of continuity and momentum for a long, thin rod may be combined to yield the characteristic equations in Lagrangian coordinates:

$$\partial u/\partial a = \partial \epsilon/\partial t \tag{1}$$

$$\partial u/\partial t = (1/\rho_0)(d\sigma/da) \tag{2}$$

where u is the particle velocity and a refers to the initial position of each layer of particles. The shift rate g, or speed of the disturbance is given by

$$g^2 = (1/\rho_0)[(\partial\sigma/\partial t)_a/(\partial\epsilon^{=}/\partial t)_a] \tag{3}$$

Defining the impact function ϕ as

$$d\phi = (1/\rho_0)(d\sigma/g) \tag{4}$$

From these equations the characteristic equations may be written as follows:

$$[\partial(u \pm \phi)/\partial t] \pm g[\partial(u \pm \phi)/\partial a] = 0 \tag{5}$$

The characteristic equations are reduced to a form which lends itself to physical interpretation while making no assumptions regarding the form of the stress-strain relation. However, the wave speed, as defined here, will vary, depending on the character of the material.

If the addition of weight to the vehicle seriously affects the capability of the system, the most efficient material for this application will be in the polymer or plastics group. Materials of this type are viscous in nature in that the stress is a function of the rate of strain, as well as the strain. In this case

$$g^2 = (1/\rho_0)(\partial\sigma/\partial\epsilon)\dot{\epsilon} + (1/\rho_0)(\partial\sigma/\partial\dot{\epsilon})\epsilon(d\ln\dot{\epsilon}/dt) \tag{6}$$

In general the term $d\ln\dot{\epsilon}/dt$ is large for problems involving impact and other types of short-duration loading. As a result, the wave speed would be expected to be not only a function of the material properties, but also the particular local acceleration. Solution of a problem of this type would be very difficult. However, it has been found that in certain materials the term $(\partial\sigma/\partial\dot{\epsilon})\epsilon$ is approximately zero for large rates of strain. These materials, such as the Polycarbonate, Lexan, exhibit what has been termed a limiting stress-strain relation above certain rates of strain.[1] The existence of such a limiting curve permits the simplification of the theory of wave propagation to the case of a strain-rate-independent material. Therefore, the velocity of propagation in this type of material will be determined by the slope of the limiting stress-strain curve.

A numerical analysis of the wave propagation problem is conveniently carried out by writing the characteristic equations in finite difference form, and by subsequent numerical integration. Solutions can be obtained for σ and u at all points on the characteristic lines.

Discussion of Results

In the experimental determination of the optimum characteristics of potential mitigating materials, the input pulses were generated by cylindrical Lexan strikers of various lengths ($\frac{1}{2}$, 1, and 2 in.) and cylindrical steel strikers 1 in. in length launched by an air gun. The projectiles were impacted against the end of a $\frac{3}{4}$-in. steel rod 30 in. long protected by various lengths of different mitigating materials. Two diametrically opposed foil-type strain gages were bonded to the rod. The results indicated that the polymer group, such as Ethocel, Teflon, Lexan, and Polyurethane, is very efficient for shock mitigation from both a weight and volume standpoint.

An IBM 7090 computer was used in the analysis of the elastic-plastic wave cancellation in energy-absorbing materials. The program was written in general form, and it can give the complete stress-time, velocity-time history of multilayered structures for any designated applied pulses. Figure 2 gives the comparison of the strain measurements from the strain gages to the theoretically calculated values for various lengths of mitigators with Lexan projectile of $\frac{1}{2}$ in. in length. Additional test were performed for various length and material of projectile and mitigators, at different velocities of impact.

The results compared very well. In addition, the results indicated for design purpose that there exists an optimum length for the mitigator. Mitigator length to projectile length ratio of 0.5 seems to give best mitigation. Any further addition in length will not have much effect on the transmitted stress level.

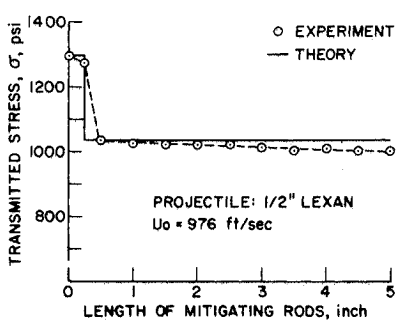

Fig. 2 Transmitted stress of various Lexan lengths.

Conclusions

In this paper, the one-dimensional elastic-plastic stress wave propagation theory using the method of characteristics is used to analyze the problem of elastic-plastic wave cancellation in energy-absorbing materials. Numerical methods were developed to analyze the propagation of the elastic-plastic stress wave in the multilayered structure that takes into account both the reflection and refraction of stress waves at the interfaces. Numerical solutions for the stress and particle velocity at any point in the structure can be obtained as functions of the time for external pressure loads of arbitrary time variation. Satisfactory agreement was obtained in the comparison of the theoretical and experimental transmitted stress results from tests conducted on steel rods

protected by varying-length mitigators and for two different projectiles.

Additional recommendations can be advanced from the results of these experimental tests: 1) the polymer group, such as Ethocel, Teflon, Lexan, and Polyurethane, is very efficient for shock mitigation from both a weight and volume standpoint; 2) for design purpose, a mitigator length to projectile length ratio of 0.5 seems to offer the optimum shock mitigation.

Reference

[1] Rand, J. L., Yang, J. C. S., and Marshall, J. M., "Dynamic Compression Testing of a Strain-Rate Material," NOLTR 65-10, Oct. 1965, U.S. Naval Ordnance Lab., Silver Springs, Md.

Anode Heat Transfer in a Constricted Tube Arc

L. A. Lukens* and F. P. Incropera†
Purdue University, West Lafayette, Ind.

Nomenclature

A	= area of the anode surface, ft²
e	= electronic charge, amp-sec
E_A	= total anode potential rise, v
Δh_A	= plasma mean enthalpy difference between the anode and asymptotic regions, Btu/lb
I	= arc current, amp
k	= Boltzmann constant, Btu/°R
$\dot{m}$	= plasma gas flow rate, lb/min
$\dot{q}_A$	= net anode heat flux, Btu/ft²-min
$\dot{q}_a$	= convective and radiative wall heat flux in the asymptotic region of the arc, Btu/ft²-min
$\dot{q}_{abl}$	= heat flux associated with anode ablation, Btu/ft²-min
$\dot{q}_e$	= anode heat flux due to electron transfer, Btu/ft²-min
$\dot{q}_{r+c}$	= anode heat flux due to plasma radiation and convection, Btu/ft²-min
$\dot{q}_\epsilon$	= radiation flux from anode surface, Btu/ft²-min
T_e	= electron temperature, °R
$U_A, U_{A'}$	= anode fall potentials, v
ϕ_A	= work function of anode material, v
ξ	= fraction of energy retained by the eletrons after traversing the anode fall region

THE need for extended periods of operation for the most severely heated component of an arc constrictor, the anode, has prompted considerable research on the complex energy exchange mechanisms occurring at this surface. In this study measurements have been performed to determine the anode heat flux for a cascade, atmospheric argon arc of the Maecker type,[1] and the results have been used to check the validity of an existing anode heat transfer model.

The anode heat transfer model of interest is one which delineates the various contributions to the total wall heat flux.[2-5] With respect to an energy balance performed on the anode surface of Fig. 1, this delineation takes the form

$$\dot{q}_A = \dot{q}_{r+c} + \dot{q}_e - \dot{q}_{abl} - \dot{q}_\epsilon \qquad (1)$$

However, from observation of negligible degradation of the anode surface and from radiation calculations for a black surface emitting at the melting temperature of copper, it is usually argued that the last two terms of Eq. (1) are negligible. The energy transferred to the anode surface by the electrons is obtained from the expression[3]

$$\dot{q}_e = (I/A)\{\xi[(1/e)(5/2)kT_e + U_A] + \phi_A\} \qquad (2)$$

where (I/e) $(5/2)$ kT_e is the energy of the electrons as they enter the anode fall region, IU_A is the energy acquired by the electrons due to acceleration through the anode fall, $I\phi_A$ denotes the condensation energy released by the electrons upon entering the anode surface, and ξ is the fraction of energy retained by the electrons subsequent to heavy-particle collisions in the fall region.

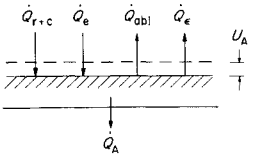

Fig. 1 Anode heat balance.

Application of this model to anode heat flux calculations requires certain additional assumptions. Those which are usually made are as follows: 1) the anode is assumed to be preceded by a fully developed (asymptotic) region with the mean enthalpy of the plasma at the anode equivalent to the mean enthalpy in the asymptotic region ($\Delta h_A = 0$). Accordingly, it is also assumed that $\dot{q}_{r+c} = \dot{q}_a$. 2) U_A is determined from the difference between the anode potential (measured with respect to the cathode) and the potential obtained by linearly extrapolating the asymptotic potential distribution to the location of the anode (Fig. 2). 3) $\xi = 1$. 4) $T_e = 18{,}000$°R and, for a copper anode surface, $\phi_A = 3.7$v. Using these assumptions with the heat transfer model and using the anode surface area of this study (2.14×10^{-3} ft²), the anode heat flux may be computed from the expression

$$\dot{q}_A = \dot{q}_a + 26.6I(5.85 + U_A) \qquad (3)$$

Measurements were performed to determine the validity of the above result for an Ar cascade arc. The constrictor was formed by stacking together individually water-cooled copper segments, each with a central bore of 1 cm and 0.632 cm in length. One of these standard segments was used as the anode, and in all test runs the anode was preceded by a sufficient number of segments to ensure the existence of an asymptotic upstream condition. The duct was operated at a pressure of 1 atm., and although measurements were performed over a wide range of laminar gas flow rates, the measured anode heat flux was found to vary only slightly (<10%) with flow rate. Accordingly, the results presented in this Note pertain only to a single flow rate ($\dot{m} = 0.03$ lb/min). The measurements included determination of the voltage, mixed-mean enthalpy, and wall heat transfer distribution in the duct from the cathode up to, and including, the anode. Details concerning the arc facility and the diagnostic procedures are provided by Lukens.[6]

Measurements were performed for five arc currents in the range from 35 to 240 amps, and the results are summarized in Table 1. The first row provides experimental results for the heat flux in the asymptotic arc region, and the second row provides the anode heat flux data. Using the measured values of $\dot{q}_a$ and U_A (tabulated in the fifth row of Table 1) with Eq. (3), a theoretical version of the anode heat flux was computed and is tabulated in the third row. Comparing the experimental and theoretical results for $\dot{q}_A$, it is evident that the former is overpredicted by a factor of approximately two.

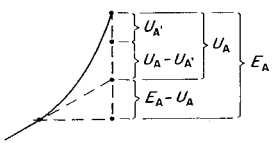

Fig. 2 Subdivision of the total anode potential.

Received May 19, 1971; revision received August 4, 1971. Supported in part by the NASA Ames Research Center under Grant NGR 15-005-129.

Index category: Plasma Dynamics and MHD.

* Graduate Student.

† Associate Professor. Member AIAA.